# Powder x-ray diffraction study of the thermoelastic martensitic transition in $Ni_2Mn_{1.05}Ga_{0.95}$

Rajeev Ranjan,[1] S. Banik,[2] S. R. Barman,[2] U. Kumar,[3] P. K. Mukhopadhyay,[3] and Dhananjai Pandey[1]
[1]*School of Materials Science and Technology, Institute of Technology, Banaras Hindu University, Varanasi-221005, India*
[2]*UGC-DAE Consortium for Scientific Research, University Campus, Khandwa Road, Indore, 452017, Madhya Pradesh, India*
[3]*LCMP, S. N. Bose National Centre for Basic Sciences, JD Block, Sector III, Salt Lake, Kolkata, 700098, West Bengal, India*
(Received 24 January 2006; revised manuscript received 8 November 2006; published 29 December 2006)

Results of temperature-dependent magnetic susceptibility and powder x-ray diffraction (XRD) measurements on $Ni_2Mn_{1.05}Ga_{0.95}$ and $Ni_{2.13}Mn_{0.87}Ga$ magnetic shape memory alloys are compared. The transformation behavior of these two alloys is found to be entirely different. Detailed LeBail and Rietveld analyses of powder XRD data of $Ni_2Mn_{1.05}Ga_{0.95}$ alloy show that the martensite phase belongs to the *Pnnm* space group with 7*M* modulation. The limits of the supercooled austenite and the superheated martensite phases have been determined by Rietveld analysis of powder XRD data recorded at close temperature intervals. It is shown that the martensite and the austenite phases coexist over ~30 K temperature range around the martensitic transition temperature. The transformation strains during cooling in [001], [010], and [100] directions are found to be −4%, +1.6%, and 2.1%, respectively, while the volume change is only 0.06%.

DOI: 10.1103/PhysRevB.74.224443 PACS number(s): 75.50.Cc, 64.70.Kb, 81.30.Kf

## I. INTRODUCTION

Currently there is enormous interest in the Ni-Mn-Ga magnetic shape memory alloy (SMA) system close to its stochiometric composition, i.e., $Ni_2MnGa$, because of its unique magnetoelastic properties.[1] Observation of magnetic-field-induced strains of 10% in this alloy system[2] makes it technologically much more promising for magnetomechanical actuator devices than other materials presently being used commercially. For example, the well known Tb-Dy-Fe alloy system (Terfenol-D) exhibits magnetostrictive strains of about 0.1% only. Similarly, the present day piezoelectric ceramics exhibit maximum strains up to 0.2%.[3] The crystal structure of the parent austenite phase in the stoichiometric $Ni_2MnGa$ compound is known to be cubic in the $Fm\bar{3}m$ space group with $L2_1$ (Heusler) atomic order.[1] It shows ferromagnetic ordering on cooling below $T_C \approx 370$ K.[1] On further cooling, it exhibits a premartensitic phase transition around 250 K, which has been attributed to the coupling of a soft transverse acoustic $TA_2$ phonon at $q=(1/3,1/3,0)$ with the homogeneous deformation associated with Zener elastic constant $c'=(c_{11}-c_{12})/2$.[4–6] Finally, on cooling below $T_m = 210$ K, it undergoes a thermoelastic martensitic phase transition.[1] Electronic structure calculations show a peak in the density of states at the Fermi level, which splits due to the redistribution of the electrons around the Fermi level in the martensite phase.[7]

The number of the martensite phases, their structures, and the sequence of their occurrence in the Ni-Mn-Ga system depend on the stoichiometry.[8–11] Chernenko *et al.*[8] have classified Ni-Mn-Ga ferromagnetic shape memory alloys into three groups based on their martensitic transition temperatures. Group I alloys, which are nearly stoichiometric, exhibit low martensitic transition temperatures as compared to the Curie temperature. This group of alloys also shows a premartensitic transition. Group II alloys have martensitic transition around room temperature but still below Curie temperature. These alloys usually exhibit stress and thermally induced intermartensitic transition also. Giant magnetic-field-induced strain is a common feature of these alloys. The group III alloys exhibit martensitic transition above the Curie temperature.

The three well-known martensite phases in this alloy system are traditionally referred to as 5*M*, 7*M*, and nonmodulated (or *NM*) phases. The 5*M* and 7*M* phases correspond to five-layer and seven-layer modulations of the $(110)_A$ planes in $[1\bar{1}0]_A$ direction, where the subscript A stands for the austenite phase.[12] The proposed modulations are based on the observation of the number of extra diffraction spots between the two parent phase spots along reciprocal lattice rows parallel to one of the $\langle 110\rangle_A$ directions on the electron diffraction patterns[10,13] and single-crystal x-ray oscillation photographs.[11–13] The cubic lattice has been reported to be distorted tetragonally with $c/a<1$ in the 5*M* phase,[1] orthorhombically in the 7*M* (Refs. 1 and 12) and tetragonally with $c/a>1$ for the *NM* phase.[14] The difference in the martensitic transition temperatures and the magnetoelastic properties of the three groups of alloys in the Ni-Mn-Ga system is believed to be due to the difference in the crystal structure of the martensite phases.[15,16] There is therefore considerable interest in understanding the structure of the Ni-Mn-Ga alloy system as a function of composition.

The splitting of the austenite 220 and the 400 peaks into two or three peaks has generally been interpreted in terms of "tetragonal"[1,17] or "orthorhombic"[13,17] distortions with 5*M* or 7*M* modulations, respectively. Wedel *et al.*[14] have assigned $I4/mmm$ and *Fmmm* space groups to the so-called tetragonally and orthorhombically distorted martensites. Neither of these two space groups has, however, been tested by comparing the observed and the calculated diffracted intensities for the martensite phases. Recently, an attempt[17] has been made to index the x-ray diffraction (XRD) peaks of the martensites of an alloy composition of the group II using these two space groups. However, a perusal of the *hkl* Miller indices given in this work[17] clearly shows that these are not consistent with the *I*- and *F*-centered lattices. The only space group that has been tested by comparing the calculated and observed intensities is *Pnnm* for the premartensite and mar-

 

tensite phases of a stoichiometric alloy.[18] There is, however, no clear understanding of the crystallographic basis of the so-called tetragonally and orthorhombically distorted martensites. In the present work, we have attempted to settle this issue in relation to the martensite phase of a nearly stoichiometric alloy composition, $Ni_2Mn_{1.05}Ga_{0.95}$, using LeBail and Rietveld analyses of the powder x-ray diffraction data.

The phase transition between the austenite and martensite phases is usually accompanied with thermal hysteresis. It is generally believed that the martensite and austenite phases coexist in the thermal hysteresis region due to superheating and supercooling effects associated with a first-order (discontinuous) phase transition. However, to the best of our knowledge, no structural evidence exists for the phase coexistence in the thermal hysteresis region of the martensitic transition in these magnetic shape memory alloys. We provide here evidence using LeBail and Rietveld analyses of powder x-ray diffraction data on a nearly stoichiometric alloy composition. It is shown that in the phase coexistence region, the powder XRD pattern exhibits triplets of peaks around the 220 and 400 austenite positions, which may be misinterpreted in terms of an orthorhombically distorted martensite phase.

This paper is organized as follows. Section II deals with the experimental details. In Secs. III A and III B, we first compare the phase transition behaviors of two representative alloy compositions belonging to group I and group II mentioned earlier using magnetic susceptibility and powder XRD measurements as a function of temperature. In Sec. III C, we analyze the structure of the so-called tetragonally distorted martensite phase for the group I alloy using $I4/mmm$ and $Pnnm$ space groups. In Sec. III D, we critically examine the structure of the same alloy in thermal hysteresis region. In Sec. III E, the issue of phase coexistence and thermal hysteresis in relation to the first-order nature of the martensitic phase transition is addressed. Section IV summarizes the main findings of the present work.

## II. EXPERIMENTAL

Polycrystalline ingots of $Ni_2Mn_{1.05}Ga_{0.95}$ and $Ni_{2.13}Mn_{0.87}Ga$ were prepared by arc melting under argon atmosphere by taking appropriate quantities of the constituent metals of 99.99% purity. The homogenization of the ingot material was done by annealing at 1100 K for 9 days. The sample was subsequently quenched in ice water. Composition of the sample was determined with energy dispersive x-ray analysis (EDAX). Powders for x-ray diffraction studies were prepared by filing the ingot. Using an optical microscope, we find that the grain size in the ingot is in the range 100–200 $\mu$m, whereas the size of the particles in the powder is in the 1–3 $\mu$m range. The powders so obtained were annealed in an inert atmosphere at 500 °C for 10 h to remove the residual stresses. Temperature-dependent powder x-ray diffraction data were collected at close temperature intervals in the 300 to 15 K range during heating and cooling using an 18 kW copper rotating anode-based Rigaku powder diffractometer fitted with a graphite monochromator in the diffracted beam and an ultralow temperature attachment. A helium closed cycle refrigerator with a cold head was used to vary the specimen temperature at a rate of 3 K per minute using a programmable temperature controller. The data collection at each temperature was started 5 min after reaching the set temperature. The temperature was stable within ±0.3 K during data collection at each temperature. The data collection in the $2\theta$ range of 20–110° was carried out in the Bragg- Brentano geometry using a scintillation counter at a step of $\Delta 2\theta = 0.02°$ and a scan rate of 2°/min. Low-field ac susceptibility, in the temperature range 80–450 K, was measured using a double-balanced coil arrangement under 26.0 Oe field and 33.33 Hz frequency.

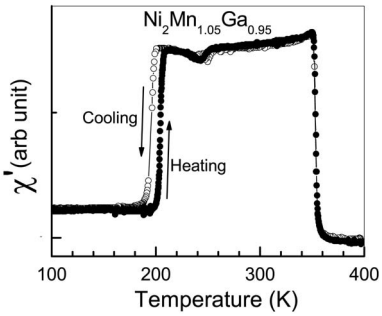


FIG. 1. Temperature variation of ac susceptibility of $Ni_2Mn_{1.05}Ga_{0.95}$ during heating and cooling.

## III. RESULTS AND DISCUSSION

### A. Magnetic behavior

Figure 1 depicts the temperature dependence of ac susceptibility ($\chi$) of $Ni_2Mn_{1.05}Ga_{0.95}$ during cooling and heating cycles. There is a sharp decrease in $\chi$ in the paramagnetic phase at the Curie temperature (=360 K).[9] $\chi$ also decreases sharply at the martensitic transition. The decrease in $\chi$ in the martensitic phase is related to the large increase in the magnetocrystalline anisotropy. From $\chi(T)$, we find the austenitic start ($A_s$), austenitic finish ($A_f$), martensitic start ($M_s$), and martensitic finish ($M_f$) temperatures to be 203, 220, 207, and 185 K, respectively. If we define the thermal hysteresis to be the difference between $(A_f+A_s)/2$ and $(M_f+M_s)/2$, the thermal hysteresis for this sample turns out to be ~15.5 K, which is in close agreement with the earlier report of 13 K hysteresis by Ma *et al.*[19,20] The small dip in $\chi$ near 250 K in Fig. 1 is characteristic of a premartensitic transition, reported earlier by Manosa *et al.*[4]

$Ni_{2.13}Mn_{0.87}Ga$ was also investigated using ac susceptibility measurements and the results are shown in Fig. 2. The Curie and the martensitic start temperatures for this alloy are found to be ~340 K and ~292 K, respectively. Further, an intermartensitic transition is observed at ~235 K. The thermal hysteresis for the martensitic and the intermartensitic transitions are found to be ~5 K and ~33 K, respectively. The transition behavior of the off-stoichiometric alloy differs from the stoichiometric alloy in the following respects: 85 K higher $M_s$ temperature, absence of any premartensitic phase and the presence of an intermartensite phase. In addition, the thermal hysteresis, corresponding to the martensitic transi-

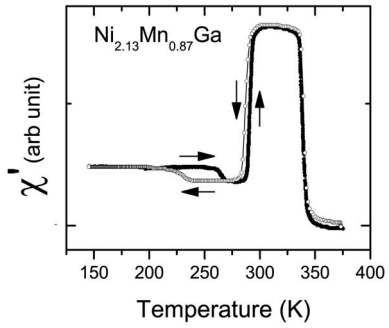


FIG. 2. Temperature variation of ac susceptibility of $Ni_{2.13}Mn_{0.87}Ga$ during heating and cooling.

tion, is significantly reduced in the off-stoichiometric alloy in comparison with the stoichiometric alloy.

### B. Temperature evolution of powder XRD pattern

Figure 3 depicts the powder XRD patterns of the austenite and the martensite phases for $Ni_2Mn_{1.05}Ga_{0.95}$. The cubic austenite phase for this alloy is stable at 300 K. The 220 austenite peak appears to have split into three and two prominent peaks at 200 K and 150 K, respectively. In addition, several new peaks are observed at these two temperatures. For comparison, we give in Fig. 4 the powder XRD patterns characteristic of the austenite, the intermediate martensite, and the low-temperature martensite phases of the off-stoichiometric alloy, recorded at 313, 238, and 223 K, respectively. Even a qualitative comparison of the XRD patterns shown in Figs. 3 and 4 reveals that the crystal structures of the martensite phases in the stoichiometric and the off-stoichiometric alloys are quite different. Having made the

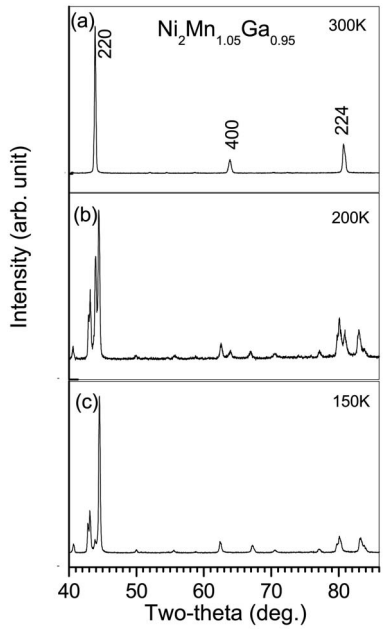


FIG. 3. Powder XRD patterns of $Ni_2Mn_{1.05}Ga_{0.95}$ at (a) 300 K, (b) 200 K, and (c) 150 K, recorded while cooling the specimen.

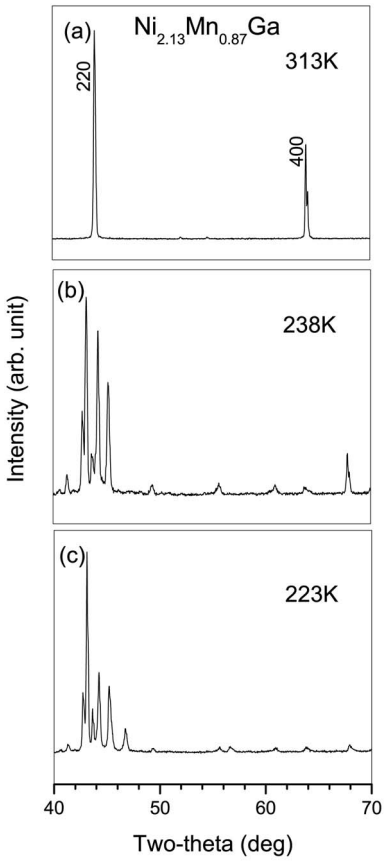


FIG. 4. Powder XRD patterns of $Ni_{2.13}Mn_{0.87}Ga$ at (a) 313 K, (b) 238 K, and (c) 223 K, recorded while cooling the specimen.

distinction between the transition behaviors of the two alloy compositions, we shall henceforth restrict ourselves to the structural investigations carried out on the nearly stoichiometric alloy only, as the structures of the intermartensite and the martensite phases of the off-stoichiometric alloy are the subject matter of a separate publication. However, the ac susceptibility and XRD data presented here for the off-stoichiometric alloy has enabled us to compare these results with those reported recently by Wang *et al.*[17] It is intriguing to note that the 300, 200, and 150 K XRD patterns for the stoichiometric alloy shown in Fig. 3 bear striking resemblance with the patterns reported by Wang *et al.*[17] for an off-stoichiometric $Ni_{2.08}Mn_{0.96}Ga_{0.96}$ alloy composition at 300, 270, and 150 K, respectively, even though the temperature variation of the magnetic susceptibility of their sample is quite different from that shown in Fig. 1. The temperature variation of the magnetic susceptibility reported by Wang *et al.* shows an intermartensitic transition that is more like the behavior of our off-stoichiometric alloy shown in Fig. 2, but the XRD patterns corresponding to the intermartensite and the martensite phases, shown in Fig. 4, are completely different from those reported by Wang *et al.* We shall return to the problems with the interpretation of the XRD data by Wang *et al.*[17] in the following sections.

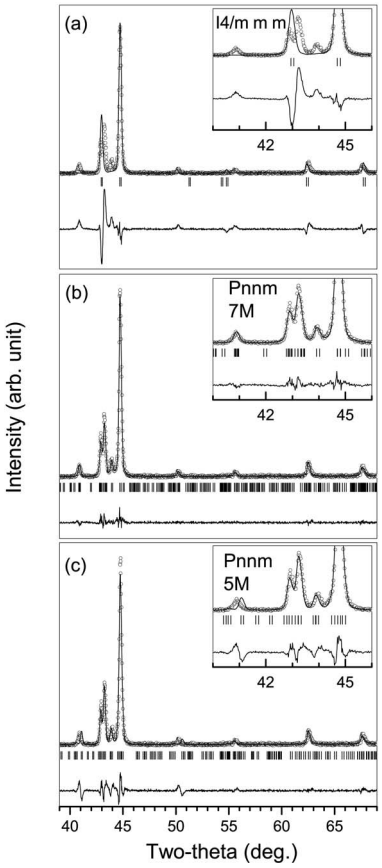


FIG. 5. LeBail fitting for the powder XRD pattern of $Ni_2Mn_{1.05}Ga_{0.95}$ at 150 K with (a) $I4/mmm$, (b) *Pnnm* with $7M$ modulated and (c) *Pnnm* with $5M$ modulated structural models. The open circles and the solid continuous lines represent observed and calculated patterns, respectively. The difference plot is shown at the bottom of each figure. Vertical bars indicate the calculated peak positions. The insets depict vertically zoomed portions in a limited $2\theta$ range.

### C. Structure of the martensite phase below 180 K in the stoichiometric alloy

As mentioned earlier, the splitting of the 220 and the 400 reflections of the austenite phase into doublets is usually taken as an evidence for a tetragonally distorted martensite phase. Wedel *et al.*[14] have assigned the space group $I4/mmm$ for such a so-called tetragonally distorted martensite phase. Wang *et al.*[17] have also assigned this space group to the martensite phase of their slightly off-stoichiometric alloy. Brown *et al.*,[18] on the other hand, have proposed a *Pnnm* space group with a seven-layered modulation ($7M$) for the martensite phase on the basis of a Rietveld analysis of the low-temperature powder neutron diffraction data on a stoichiometric alloy composition.

We shall first make a choice between the $I4/mmm$ and *Pnnm* space groups for the martensite phase in the stoichiometric alloy using LeBail fitting procedure available with the FULLPROF software package.[21] This is an easy and efficient way to test the plausibility of the space groups. The LeBail fit for the $I4/mmm$ space group is shown in Fig. 5(a). As can be seen from this figure, there is significant mismatch between the observed and the calculated patterns for this space group. The zoomed pattern in the inset clearly reveals that what appears as a doublet on a reduced $2\theta$ scale is in fact a triplet, which cannot be explained in terms of a tetragonal distortion of the cubic austenite unit cell. Further, the weak reflections near 50° and 55°, which have been indexed by Wang *et al.* as 311 and 222, show mismatch between the observed and the calculated peak positions, thereby suggesting that they do not owe their origin to the tetragonal distortion of the parent austenite lattice. As we shall see later on, these two reflections, along with the weak reflection near $2\theta$=40.50, are in fact superlattice reflections, which result from a seven-layer ($7M$) modulation.

Figure 5(b) depicts the LeBail fit for the *Pnnm* space group. It is evident that this space group nicely accounts for all the strong as well as the weak reflections. Further, refined unit cell parameters [$a_M$=4.209(2) Å, $b_M$=29.270(5) Å, and $c_M$=5.562(3) Å] reveal that $a_M \approx \sqrt{2}a_A$, $b_M \approx 7\sqrt{2}a_A$, and $c_M \approx a_A$, where $a_A$ is the cubic austenite cell parameter, confirming a seven-layer ($7M$) modulation in the $[1\bar{1}0]$ direction. We also considered *Pnnm* space group with five-layer ($5M$) modulation instead of seven layer ($7M$), as proposed by some workers[17] for the so-called tetragonally distorted martensite. It was found that although the strong peaks can be accounted for using $5M$ modulation, there is a distinct mismatch between the observed and the calculated peak positions for the superlattice reflections [see, e.g., the superlattice peak at $2\theta \approx 41°$ in the inset of Fig. 5(c)].

Having identified the correct space group (*Pnnm*), we carried out Rietveld refinement of the structure of the martensite phase of our nearly stoichiometric alloy. The asymmetric unit of this structure consists of four Mn atoms, four Ni atoms, and four Ga atoms. Mn1 occupies the $2a$ Wyckoff position at (0,0,0). Mn2, Mn3, and Mn4 occupy the $4g$ site ($xy0$) at $(0+\delta x_{Mn1},\ 1/7+\delta y_{Mn1},0)$, $(0+\delta x_{Mn2},\ 2/7+\delta z_{Mn2},0)$, and $(0+\delta x_{Mn3},\ 3/7+\delta y_{Mn3},0)$, respectively. Ni1 occupies the $4f$ Wyckoff site (1/2 0 z) at $(0.5,0,0.25+\delta z_{Ni1})$; Ni2, Ni3, and Ni4 occupy the $8h$ Wyckoff site ($xyz$) at $(0.5+\delta x_{Ni2},\ 1/7+\delta y_{Ni2},\ 0.25+\delta z_{Ni2})$, $(0.5+\delta x_{Ni3},\ 2/7+\delta y_{Ni3},\ 0.25+\delta z_{Ni3})$, and $(0.5+\delta x_{Ni3},\ 3/7+\delta y_{Ni3},\ 0.25+\delta z_{Ni3})$ respectively. Ga1 occupies the $2b$ site at (0,0,0.5); Ga2, Ga3, and Ga4 occupy the $4g$ Wyckoff site ($xy0$) at $(0+\delta x_{Ga2},\ 1/7+\delta y_{Ga2},0.5)$, $(0+\delta x_{Ga3},\ 2/7+\delta y_{Ga3},0.5)$, and $(0+\delta x_{Ga4},\ 1/7+\delta y_{Ga4},0.5)$, respectively. The various $\delta$ are the space group allowed refinable coordinates. Although the space group *Pnnm* allows for independent refinement of the $y$ and $z$ coordinates of most of the atoms in the asymmetric unit, we have fixed the various $\delta y$ and $\delta z$ to zero following Brown *et al.*[18] This is consistent with the shuffling model proposed by earlier workers, in which the atoms in the neighboring $(\bar{1}10)$ planes are assumed to shift in the [110] direction of the austenite cell, thereby resulting in a long-range modulation along $[\bar{1}10]$ direction.[12]

The FULLPROF package[21] was used for Rietveld refinement also. Background was fitted using linear interpolation between the data points. Pseudo-Voigt profile shape function was selected to model the line shapes of the various Bragg

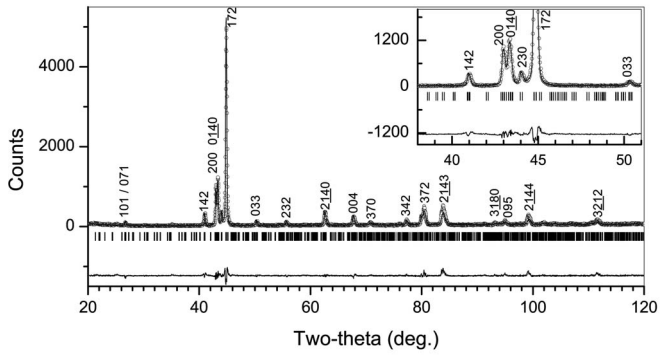


FIG. 6. Observed (open circles), calculated (continuous line), and difference plots after Rietveld refinement of $Ni_2Mn_{1.05}Ga_{0.95}$ structure at 15 K with *Pnnm* space group and 7*M* modulation. The vertical bars represent Bragg positions. The inset depicts a vertically zoomed plot in a limited $2\theta$ range. The indices of the Bragg reflections are also mentioned.

reflections. The starting values of the positional coordinates were taken from Brown *et al.*[18] During the refinement scale factor, zero correction, shape parameters, half-width parameters, lattice parameters, positional coordinates, and isotropic thermal parameters were varied. Figure 6 depicts the observed, calculated, and the difference plots obtained after the Rietveld refinement. The fit between the observed and the calculated plots is quite good, suggesting the correctness of the structural model for the martensite phase. The inset in Fig. 6 shows a portion of the plot in the $2\theta=39°-51°$ range. It is evident that the orthorhombic *Pnnm* space group with 7*M* modulated structure not only accounts nicely for the doublet structure of the peak at $2\theta=43°$ but also the weak peak around $2\theta=44°$. Both these features were not explicable in terms of the so-called tetragonally distorted structure of the martensite phase. We can thus conclude that the 7*M* modulated structure model in the *Pnnm* space group, proposed earlier by Brown *et al.*[18] describes satisfactorily all the features of the powder diffraction data of the martensite phase in our nearly stoichiometric alloy composition.

The striking similarity of the XRD data of Wang *et al.* for the martensite phase at 150 K with our XRD data at 150 K suggests that the structure of the martensite phase of Wang *et al.*'s composition may also belong to the *Pnnm* space group, and not to the $I4/mmm$ space group with 7*M* or 5*M* periodicity. It may also be noted that the indices assigned to various XRD peaks by Wang *et al.* using tetragonal unit cell for the martensite phase are not consistent with the body (*I*)-centering for which $h+k+1$ should always be an even number. Thus, for example, the assignment of 311 and 214 indices by Wang *et al.* to two of the XRD peaks is obviously inconsistent with the *I*-centered space group.

The refined structural parameters for the martensite phase using *Pnnm* space group are given in Table I. The refined coordinates and the cell parameters are in good agreement with those reported by Brown *et al.*[18] using powder neutron diffraction data.

TABLE I. Refined structural parameters in *Pnnm* space group of the martensite phase of $Ni_2Mn_{1.05}Ga_{0.95}$ at 15 K.

| Atoms | *X* | *Y* | *Z* | *B* (Å$^2$) |
|---|---|---|---|---|
| Ni1 | 0.5 | 0.0 | 0.25 | 0.0(3) |
| Ni2 | 0.48(2) | 1/7 | 0.25 | 0.2(3) |
| Ni3 | 0.54(1) | 2/7 | 0.25 | 0.1(3) |
| Ni4 | 0.43(1) | 3/7 | 0.25 | 0.1(3) |
| Mn1 | 0.0 | 0.0 | 0.0 | 0.3(2) |
| Mn2 | −0.03(2) | 1/7 | 0.0 | 0.03(10) |
| Mn3 | 0.05(1) | 2/7 | 0.0 | 0.2(3) |
| Mn4 | −0.05(2) | 3/7 | 0.0 | 0.1(3) |
| Ga1 | 0.0 | 0.0 | 0.5 | 0.8(3) |
| Ga2 | −0.04(2) | 1/7 | 0.5 | 0.4(3) |
| Ga3 | 0.04(1) | 2/7 | 0.5 | 0.5(3) |
| Ga4 | −0.06(1) | 3/7 | 0.5 | 0.7(3) |
| $a=4.2115(3)$ Å, $b=29.253(2)$ Å, $c=5.5321(4)$ Å | | | | |
| $\chi^2=2.6$ | | | | |

### D. Structure of $Ni_2Mn_{1.05}Ga_{0.95}$ in the temperature range 185 K < *T* < 215 K

The powder XRD patterns of our nearly stoichiometric alloy shows the presence of three peaks around the 220 and 400 austenite positions in the temperature range 185 K < *T* < 215 K. As mentioned earlier in Sec. III B, the 200 K XRD pattern showing triplets of peaks in Fig. 3(b) resembles the 270 K pattern reported by Wang *et al.*,[17] who have interpreted this in terms of an orthorhombic distortion of the austenite phase[17] in the space group *Fmmm*.[14,17] We therefore first analyzed the 200 K pattern shown in Fig. 3(b) by the LeBail technique using the *Fmmm* space group. The pronounced mismatch between the observed and the calculated patterns shown in Fig. 7(a) clearly indicates the incorrectness of this space group. Only the three strong peaks are exactly indexable with this space group.

The triplet of peaks around the austenite reflections in Fig. 3 can also be due to coexistence of the austenite and the martensite phases in and around the temperature range of thermal hysteresis. To verify this hypothesis, we again used the LeBail technique. The result of this two-phase refinement is shown in Fig. 7(b). The nice fit between the calculated and the observed profiles confirms the phase coexistence model. Having confirmed the phase coexistence model using the LeBail technique, we also carried out a Rietveld refinement to determine the mole fractions of the austenite ($Fm3m$) and the martensite (*Pnnm*) phases, which were found to be 37% and 63%, respectively, at 200 K.

Our results clearly suggest that the triplet-like features around the 220 and 400 austenite peaks can arise due to the coexistence of austenite and the martensite phases and may not necessarily be linked with the orthorhombic distortion of the cubic austenite phase in the *Fmmm* space group, assumed by Wang *et al.*[17] in the interpretation of their 270 K XRD pattern. In fact, a careful perusal of the indices attributed to the *Fmmm* space group in Ref. 17 for the intermediate martensite phase at 270 K shows an apparent contradiction with

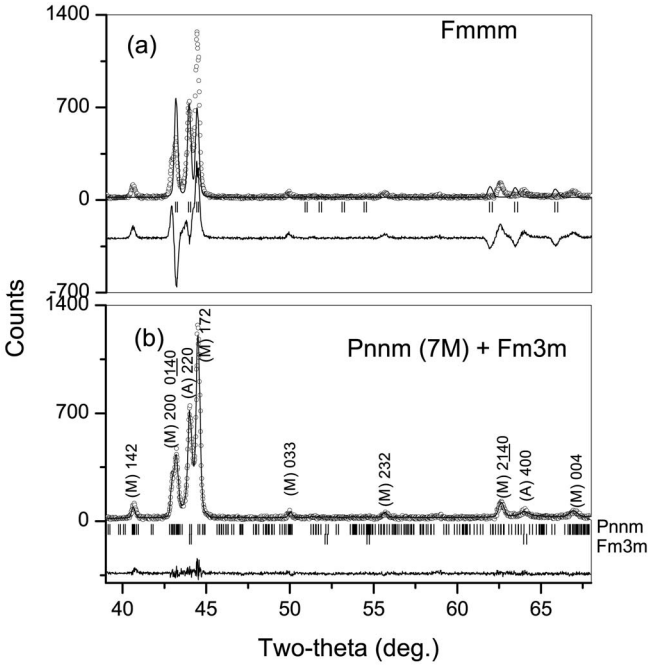


FIG. 7. LeBail fitting of the XRD pattern of $Ni_2Mn_{1.05}Ga_{0.95}$ at 200 K with (a) space group *Fmmm* and (b) martensite (*Pnnm* space group with 7*M* modulation) + austenite (*Fm*3*m* space group) phase coexistence model. The observed and the calculated patterns are shown with open circles and continuous lines. The difference profiles are shown at the bottom of each figure. The vertical bars represent Bragg positions. In (b) the upper bars correspond to the *Pnnm* space group while the lower bars correspond to the *Fm*3*m* space group. The indices of the Bragg reflections are written on top of the respective peaks. "M" and "A" represent peaks corresponding to the martensite and austenite phases, respectively.

the *F*-centered lattice for which the Miller indices should be all odd or all even integers. For example, the indices such as 214, assigned to one of the XRD peaks in Ref. 17, are inconsistent with the *F*-centered lattice and hence with the *Fmmm* space group also.

### E. Phase coexistence and thermal hysteresis

The phase coexistence model, discussed in the previous section, was further confirmed by monitoring the temperature evolution of the 220 and 400 austenite profiles at close temperature intervals during heating and cooling cycles (see Fig. 8 for the cooling cycle). It is evident from this figure that the martensite peaks (marked with *M*) appear around 215 K and coexist with the austenite peaks (marked with *A*). With decreasing temperature, the intensity of the martensite peaks remains nearly constant in the 210 to 206 K range and then starts growing suddenly at $T \leq 204$ K with a concomitant decrease in the intensity of the austenite peaks. The austenite peaks disappear around 185 K. The small peak near the 220 austenite peak position in Fig. 8(a) below 185 K is a superlattice peak arising from seven-layer modulation (7*M*). It is evident from this evolution of the profiles that the austenite and the martensite phases coexist in the $180\ \text{K} < T$

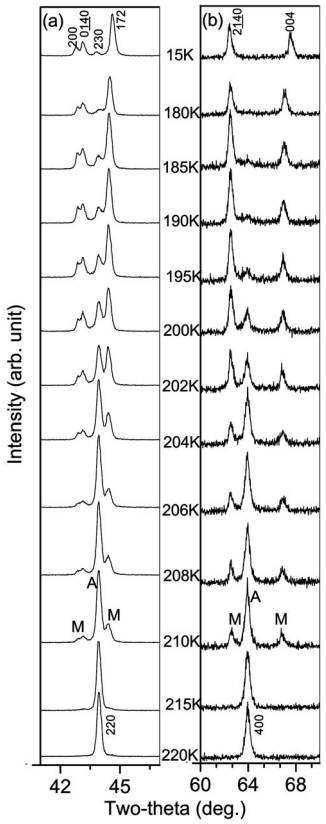


FIG. 8. Evolution of (a) 220 and (b) 400 Bragg profiles as a function of temperature during cooling cycle. "M" and "A" represent the Bragg peaks due to the 7*M* martensite and austenite phases, respectively. Indices are with respect to the orthorhombic 7*M* cell.

$< 215$ K temperature interval. The $M_s$ and the $M_f$ temperatures, obtained from the Rietveld analysis of the XRD data, are ~215 K and ~185 K. A similar study for the heating cycle gave $A_s$ and $A_f$ temperatures as 190 K and 230 K. The austenite XRD peaks are observed up to about 190 K during cooling while the martensite phase peaks are present up to about 225 K during heating. The average of the martensite transition temperatures obtained by magnetic susceptibility measurements during the heating and cooling cycles is $T_m$ ~200 K. Thus the austenite phase exists in the supercooled

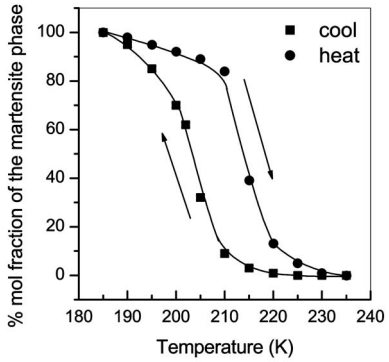


FIG. 9. Variation of mol fraction of the martensite phase, as obtained by Rietveld refinement, with temperature during heating (filled circles) and cooling cycles (filled squares)

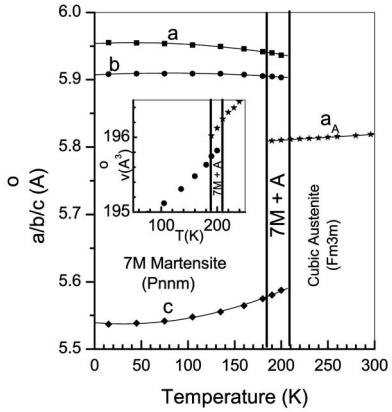


FIG. 10. Temperature variation of $a$, $b$, $c$, of $Ni_2Mn_{1.05}Ga_{0.95}$ in the austenite ("A") and the martensite ("M") phase regions for the cooling cycle. The $a$ and $b$ parameters plotted in this figure are scaled with $\sqrt{2}$ and $\sqrt{2}/7$, respectively, for easy comparison with the lattice parameter of the austenite phase. The inset shows a discontinuous jump in the unit cell volume.

state up to $(T_m-10)$ K, while the martensite phase persists up to $(T_m+25)$ K. Figure 9 depicts the evolution of the percentage mole fraction of the martensite phase, as obtained by Rietveld refinement at each temperature, during cooling and heating cycles. The phase coexistence and thermal hysteresis shown in this figure is due to the first-order nature of the austenite-martensite phase transition, and is consistent with the thermal hysteresis in the magnetic susceptibility measurements. This is also supported by the discontinuous change in the lattice parameters at the transition temperature shown in Fig. 10. The lattice strains in the [001], [010], and [100] directions are found to be −4.0%, +1.6%, and +2.1%, respectively. The unit cell volume also shows a small (0.06%) but distinct discontinuous change. Both the narrow coexistence region (~30 K) and small discontinuous change in volume at $T_m$ confirm the thermoelastic nature of the martensitic transition which is quite distinct from the nonthermoelastic martensitic transitions, which are usually characterized by one order of magnitude larger coexistence regions.[22] In fact, the necessary and sufficient condition for a cubic to tetragonal martensitic transition to exhibit self-accommodation and shape memory effect is conservation of the unit cell volume.[23] Different SMA materials with cubic austenitic phase exhibit a small volume change of 0.1 to 0.4%. Present results show that $Ni_2MnGa$, which is a ferromagnetic SMA, exhibits small volume change across the martensitic transition in agreement with conditions of self-accommodation. This result is also in agreement with the theoretical prediction of hardly any change in unit cell volume (0.03%) based on full-potential linear-augmented plane-wave method (FPLAPW) calculations.[24]

## IV. CONCLUSIONS

The main findings of the present work may be summarized as follows: (i) The powder XRD pattern of the martensite phase of a nearly stoichiometric $Ni_2Mn_{1.05}Ga_{0.95}$ alloy exhibits the so-called tetragonal distortion of the cubic lattice, but its correct space group is *Pnnm* (Ref. 18) with a 7*M* type modulation, and not $I4/mmm$.[13,17] (ii) The triplets of powder XRD peaks observed around the cubic 220 and 400 reflections in the thermal hysteresis region is not due to an orthorhombic distortion of the cubic lattice[17] but results from a coexistence of the austenite and the martensite phases. (iii) The austenite and the martensite phases coexist in the temperature range $185\ \text{K} < T < 215\ \text{K}$ during cooling and $190\ \text{K} < T < 230\ \text{K}$ during heating. The maximum supercooling and superheating temperatures of the austenite and martensite phases responsible for the thermal hysteresis are found to be $(T_m\text{-}10)$ K and $(T_m+25)$ K, where $T_m \sim 200$ K. (iv) The transformation strains during cooling in [001], [010], and [100] directions are found to be −4%, +1.6%, and 2.1%, respectively. However, the percentage volume change at the transition temperature is found to be very small (~0.06%), as expected for the thermoelastic martensites.

## ACKNOWLEDGMENTS

We thank N. P. Lalla, A. M. Awasthi, D. M. Phase, V. Ganesan, and V. Sathe for help in characterization studies. The Department of Science and Technology, Government of India, is thanked for supporting the work. S.B. is thankful to the Council for Scientific and Industrial Research for financial support.

[1] P. J. Webster, K. R. A. Ziebeck, S. L. Town, and M. S. Peak, Philos. Mag. B **49**, 295 (1984).
[2] A. Sozinov, A. A. Likhachev, N. Lanska, and K. Ullakko, Appl. Phys. Lett. **80**, 1746 (2002); S. J. Murray, M. Marioni, S. M. Allen, R. C. O'Handley, and T. A. Lograsso, *ibid.* **77**, 886 (2000).
[3] S.-E. Park and T. R. Shrout, J. Appl. Phys. **82**, 1804 (1997).
[4] L. Manosa, A. Planes, J. Zaretsky, T. Lograsso, D. L. Schlagel, and C. Stassis, Phys. Rev. B **64**, 024305 (2001).
[5] U. Stuhr, P. Vorderwisch, V. V. Kokorin, and P.-A. Lindgard, Phys. Rev. B **56**, 14360 (1997).
[6] A. Zheludev, S. M. Shapiro, P. Wochner, A. Schwartz, M. Wall, and L. E. Tanner, Phys. Rev. B **51**, 11310 (1995).
[7] P. J. Brown, A. Y. Bargawi, J. Crangle, K.-U. Neumann, and K. R. A. Ziebeck, J. Phys.: Condens. Matter **10**, 4715 (1999).
[8] V. A. Chernenko, E. Cesari, V. V. Kokorin, and I. N. Vitenko, Scr. Metall. Mater. **33**, 1239 (1995).
[9] A. N. Vasilev, A. D. Bozhko, V. V. Khovailo, I. E. Dikshtein, V. G. Shavrov, B. D. Buchelnikov, M. Matsumoto, S. Suzuki, T. Takagi, and J. Tani, Phys. Rev. B **59**, 1113 (1999).
[10] J. Pons, V. A. Chernenko, R. Santamarta, and E. Cesari, Acta Mater. **48**, 302 (2000).
[11] N. Lanska, O. Söderberg, A. Sozinov, Y. Ge, K. Ullakko, and V. K. Lindroos, J. Appl. Phys. **95**, 8074 (2004).

[12] V. V. Martinov and V. V. Kokorin, J. Phys. III **2**, 739 (1992).
[13] A. Sozinov, A. A. Likhachev, N. Lanska, and K. Ullakko, Appl. Phys. Lett. **80**, 1746 (2002).
[14] B. Wedel, M. Suzuki, Y. Murakami, C. Wedel, T. Suzuki, D. Shindo, and K. Itagaki, J. Alloys Compd. **290**, 137 (1999).
[15] S. J. Murray, M. A. Marioni, A. M. Kukla, J. Robinson, R. C. O'Handley, and S. M. Allen, J. Appl. Phys. **87**, 5774 (2000).
[16] A. Sozinov, A. A. Likhachev, N. Lanska, K. Ullakko, and U. K. Lindroos, J. Phys. IV **112**, 955 (2003).
[17] W. H. Wang, Z. H. Liu, J. Zhang, J. L. Chen, G. H. Wu, W. S. Zhan, T. S. Chin, G. H. Wen, and X. X. Zhang, Phys. Rev. B **66**, 052411 (2002).
[18] P. J. Brown, J. Crangle, T. Kanomata, M. Matsumoto, K.-U. Neumann, B. Ouladdiaf, and K. R. A. Ziebeck, J. Phys.: Condens. Matter **14**, 10159 (2002).
[19] Y. Ma, S. Awaji, K. Watanabe, M. Matsumoto, and N. Kobayashi, Appl. Phys. Lett. **76**, 37 (2000).
[20] Y. Ma, S. Awaji, K. Watanabe, M. Matsumoto, and N. Kobayashi, Solid State Commun. **113**, 671 (2000).
[21] Rodiguez J. Carvajal, FULLPROF, Laboratoire Leon Brillouin (CEA-CNRS), France.
[22] C. M. Wayman, in *Solid State Phase Transformations*, edited by H. I. Aranson, D. E. Loughlin, R. F. Sekerka, and C. M. Wayman (Met. Soc. of AIME, Warrendale, PA, 1982), p. 1119.
[23] K. Bhattacharya, *Microstructure of Martensite: Why It Forms and How It Gives Rise to Shape Memory Effect* (Oxford University Press, Oxford, 2003).
[24] S. R. Barman, S. Banik, and A. Chakrabarti, Phys. Rev. B **72**, 184410 (2005).